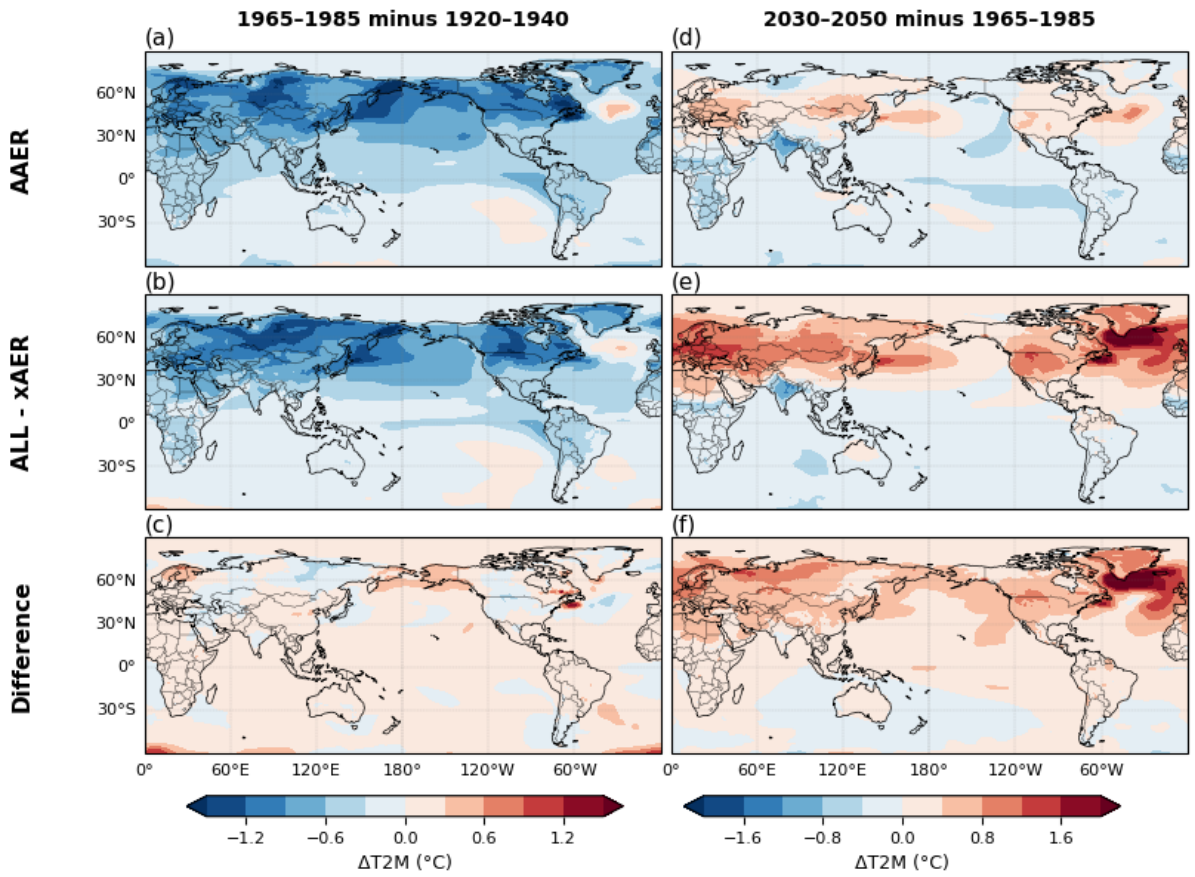

Figure S1. Sensitivity of the JJA near-surface air temperature response to ensemble size, using the full available ensemble members for each experiment. Differences in JJA mean near-surface air temperature (ΔT2M; °C) are shown for 1965–1985 relative to 1920–1940 (left) and 2030–2050 relative to 1965–1985 (right), for (a, d) AAER, (b, e) ALL−xAER, and (c, f) the difference between them (ALL−xAER minus AAER).

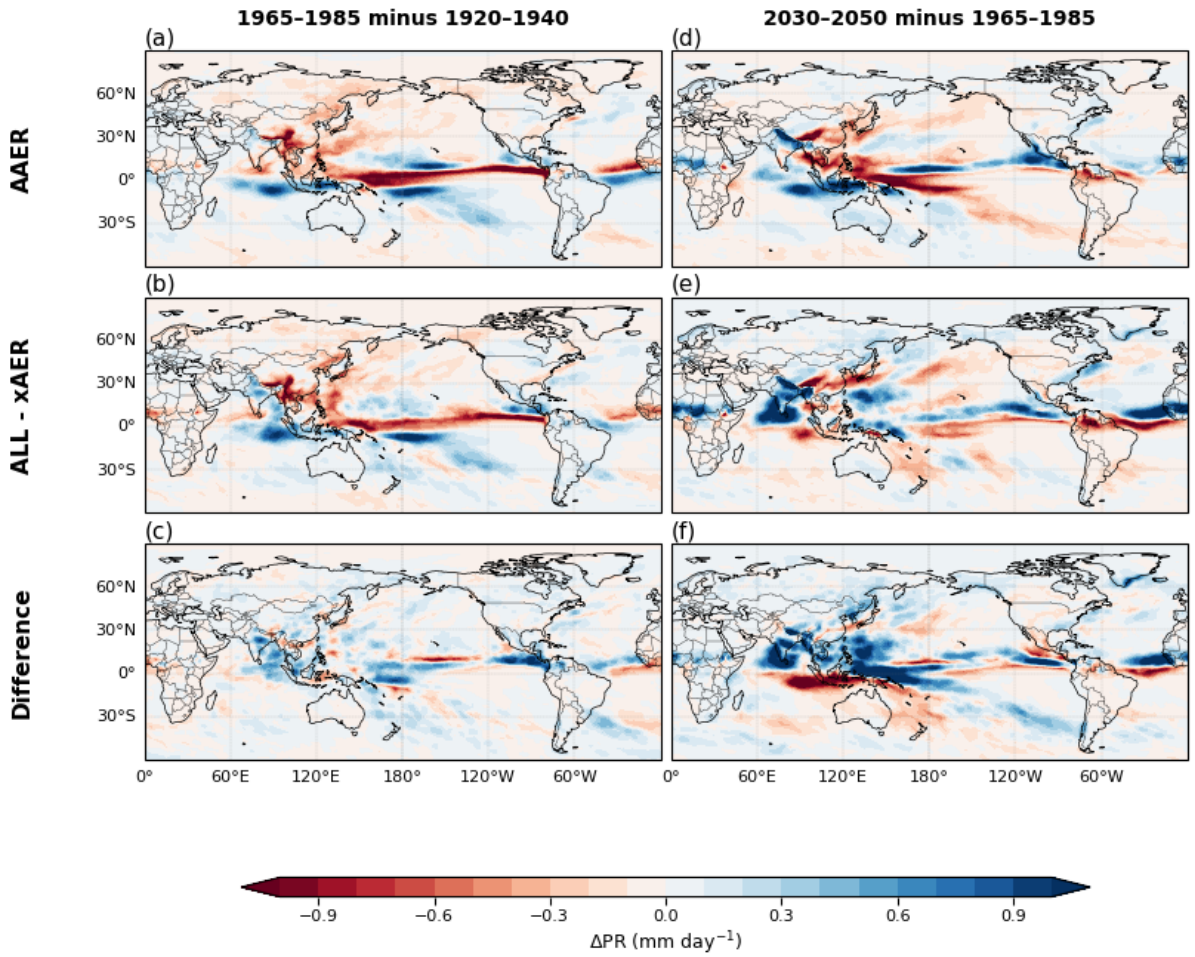

Figure S2. Sensitivity of the JJA precipitation response to ensemble size, using the full available ensemble members for each experiment. Differences in JJA mean precipitation (ΔPR; mm day−1) are shown for 1965–1985 relative to 1920–1940 (left) and 2030–2050 relative to 1965–1985 (right), for (a, d) AAER, (b, e) ALL−xAER, and (c, f) the difference between them (ALL−xAER minus AAER).

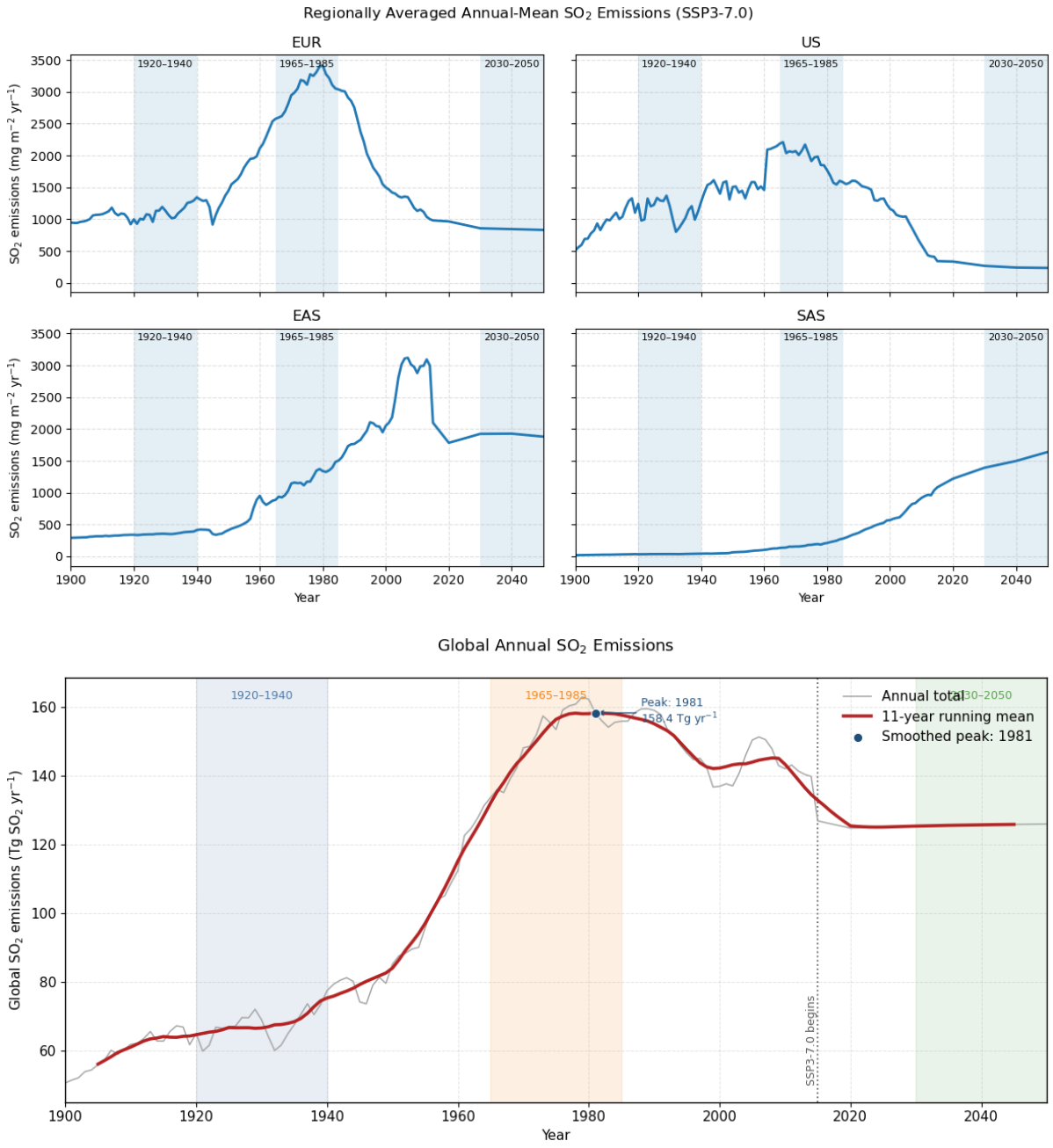

Figure S3. Evolution of annual-mean SO_2 emissions over the historical and SSP3-7.0 periods. Regionally averaged SO_2 emissions are shown for Europe (EUR), the United States/North America (US), East Asia (EAS), and South Asia (SAS) in units of mg m^{-2} yr^{-1}. Global annual SO_2 emissions are shown in Tg SO_2 yr^{-1}, with the annual total in grey and the 11-year running mean in red; the blue marker indicates the maximum of the smoothed global time series. The vertical dotted line marks the beginning of SSP3-7.0 forcing in 2015. Shaded bands indicate the three analysis periods used in this study: 1920–1940, 1965–1985, and 2030–2050. SO_2 emissions are used as a representative indicator of the temporal and geographical evolution of anthropogenic aerosol forcing.

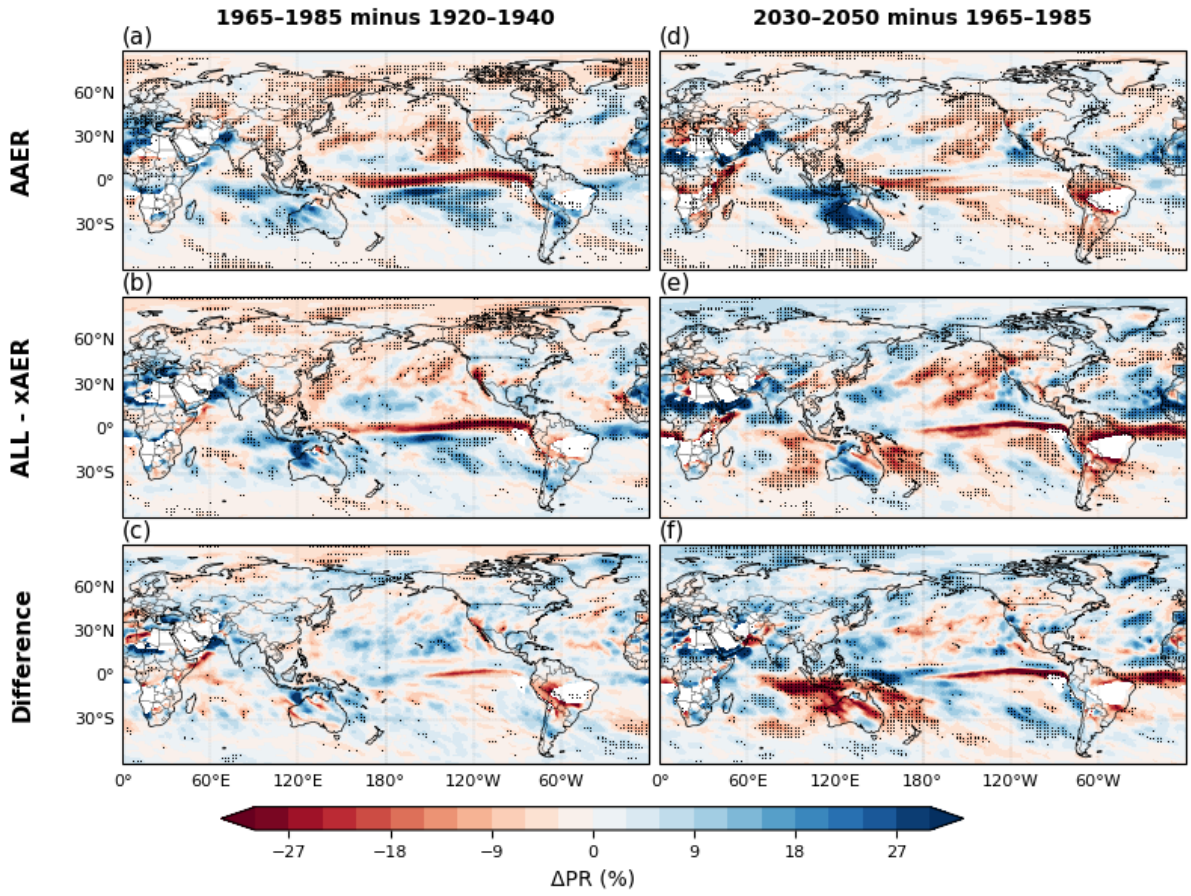

Figure S4. Difference in JJA mean precipitation percentage (%) of the corresponding ALL baseline climatology between two different periods: 1965–1985 relative to 1920–1940 (left) and 2030–2050 relative to 1965–1985 (right). (a), (d) AAER, (b), (e) ALL−xAER, and (c), (f) the difference between them (ALL−xAER minus AAER). Stippling indicates anomalies that are statistically significant at the 95% confidence level.

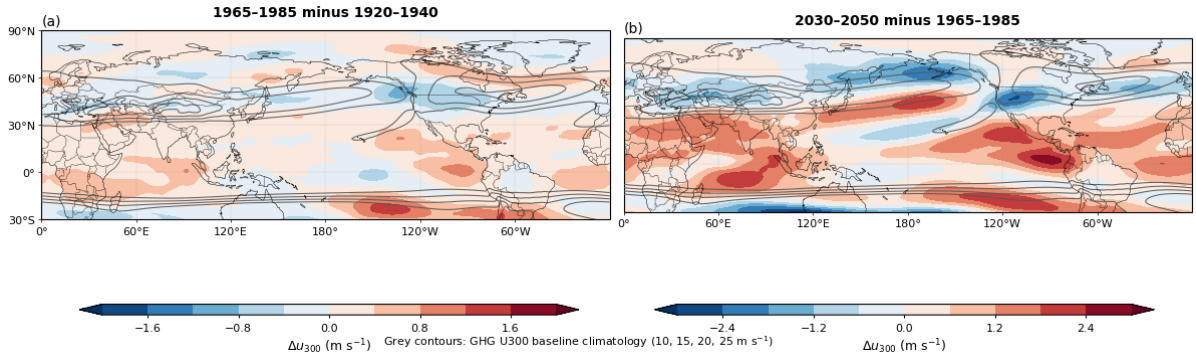

Figure S5. Changes in JJA mean zonal wind at 300 hPa (shading, unit: m s^{-1}) in the GHG-only experiment for (a) 1965–1985 relative to 1920–1940 and (b) 2030–2050 relative to 1965–1985. Grey contours show the corresponding GHG JJA mean 300-hPa zonal-wind climatology during the baseline periods (1920–1940 in panel a and 1965–1985 in panel b), with contour levels of 10, 15, 20, and 25 m s^{-1}.

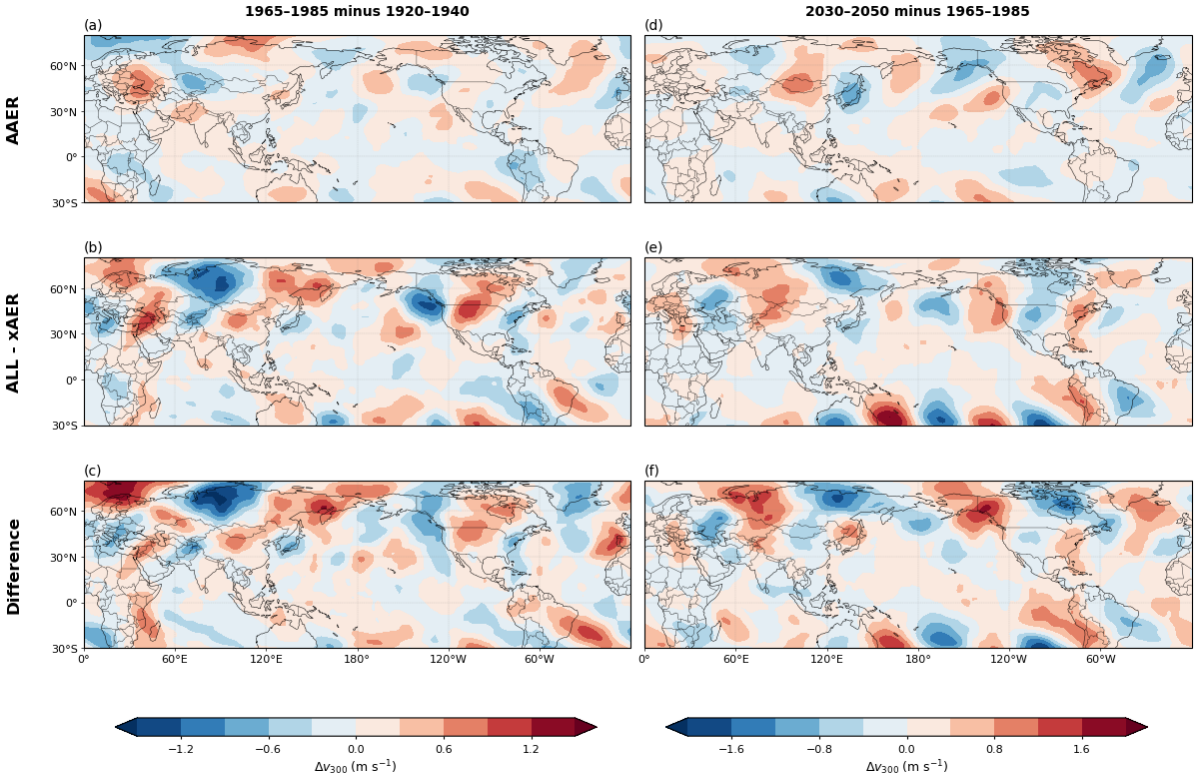

Figure S6. Changes in JJA mean meridional wind at 300 hPa (shading, unit: m s^{-1}) between two different periods: 1965–1985 relative to 1920–1940 (left) and 2030–2050 relative to 1965–1985 (right) for the (a), (d) AAER, (b), (e) ALL−xAER, and (c), (f) difference between them (ALL−xAER minus AAER).

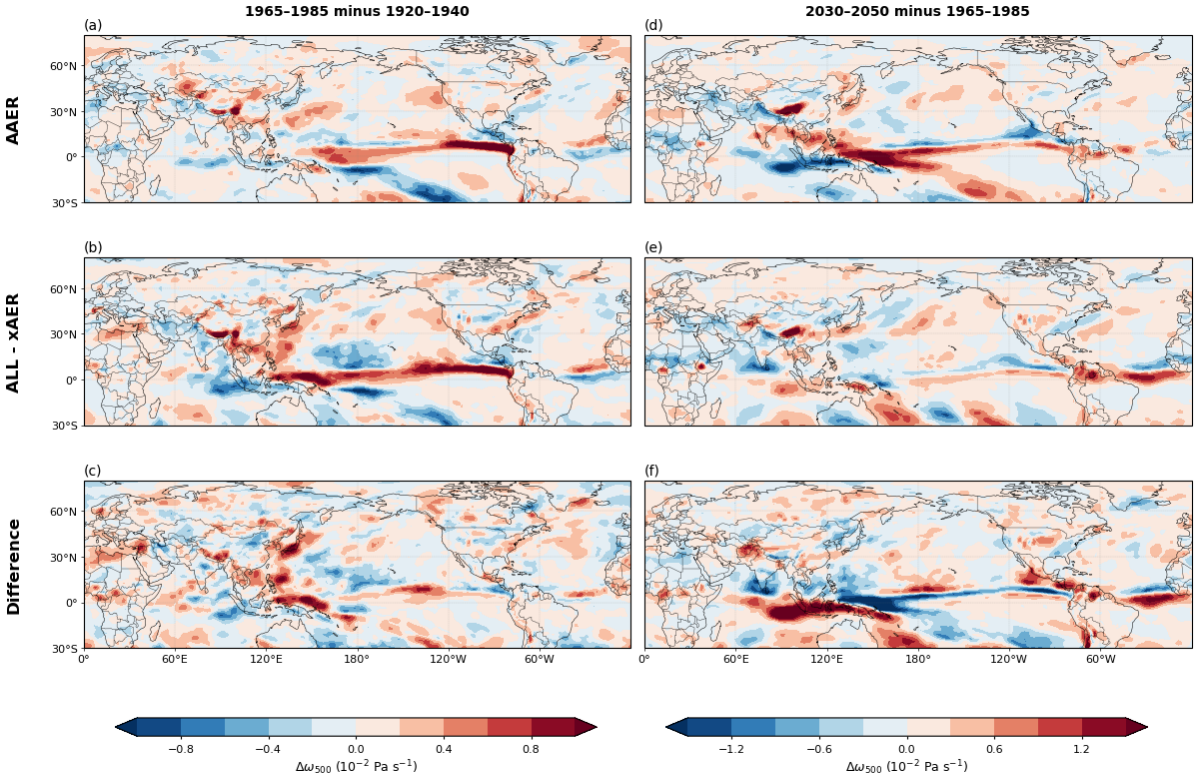

Figure S7. Changes in JJA mean pressure vertical velocity at 500 hPa (shading, unit: Pa s^{-1}) between two different periods: 1965–1985 relative to 1920–1940 (left) and 2030–2050 relative to 1965–1985 (right) for the (a), (d) AAER, (b), (e) ALL−xAER, and (c), (f) difference between them (ALL−xAER minus AAER). Negative values indicate anomalous ascent and positive values indicate anomalous descent.

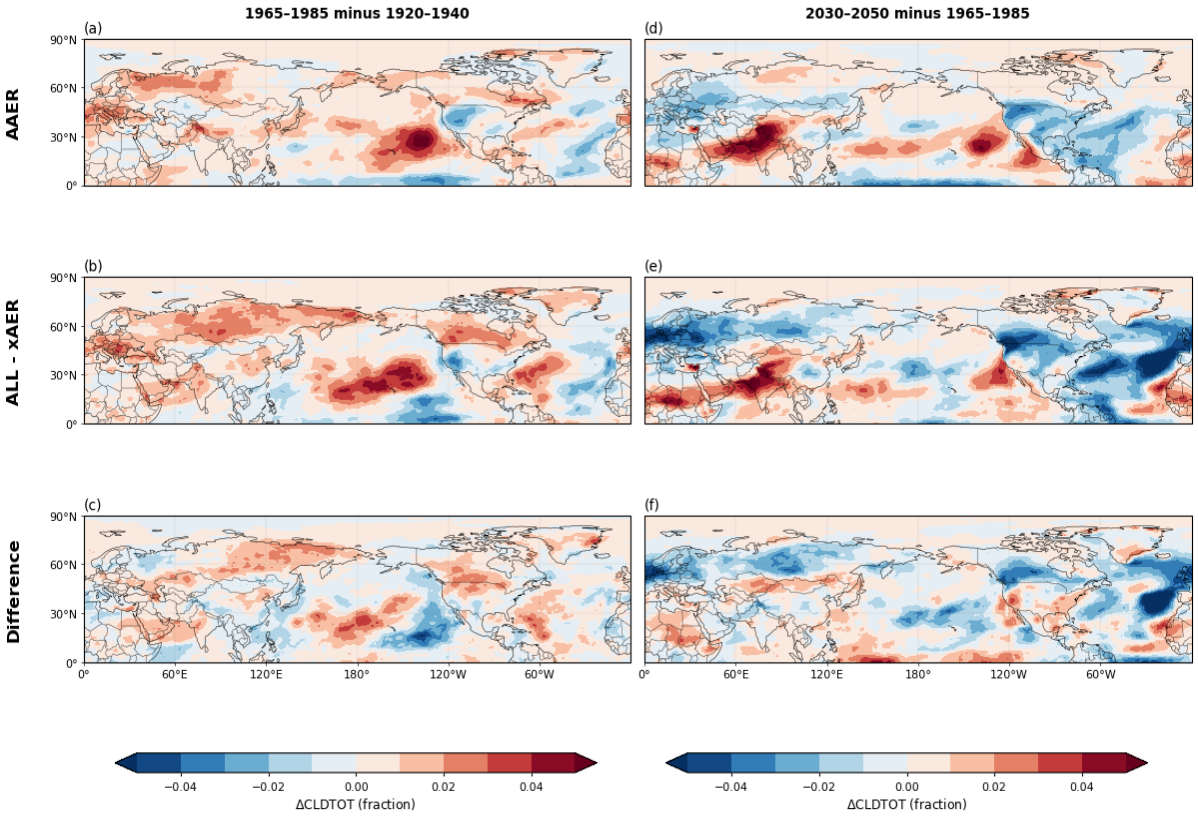

Figure S8. Changes in JJA mean total cloud fraction (CLDTOT; shading, unit: unitless fraction) between two different periods: 1965–1985 relative to 1920–1940 (left) and 2030–2050 relative to 1965–1985 (right) for the (a), (d) AAER, (b), (e) ALL−xAER, and (c), (f) difference between them (ALL−xAER minus AAER). Positive anomalies indicate increased total cloud fraction, whereas negative anomalies indicate reduced total cloud fraction.

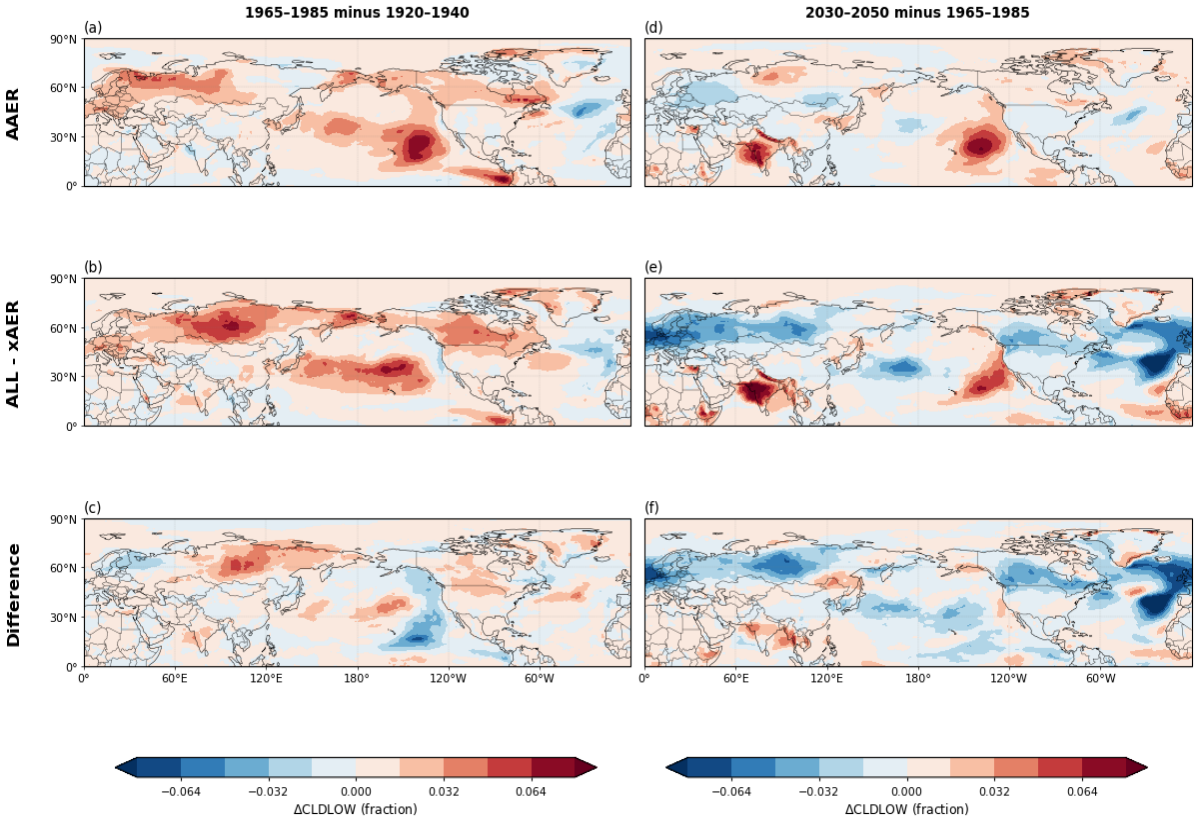

Figure S9. Changes in JJA mean low-cloud fraction (CLDLOW; shading, unit: unitless fraction) between two different periods: 1965–1985 relative to 1920–1940 (left) and 2030–2050 relative to 1965–1985 (right) for the (a), (d) AAER, (b), (e) ALL−xAER, and (c), (f) difference between them (ALL−xAER minus AAER). Positive anomalies indicate increased low-cloud fraction, whereas negative anomalies indicate reduced low-cloud fraction.

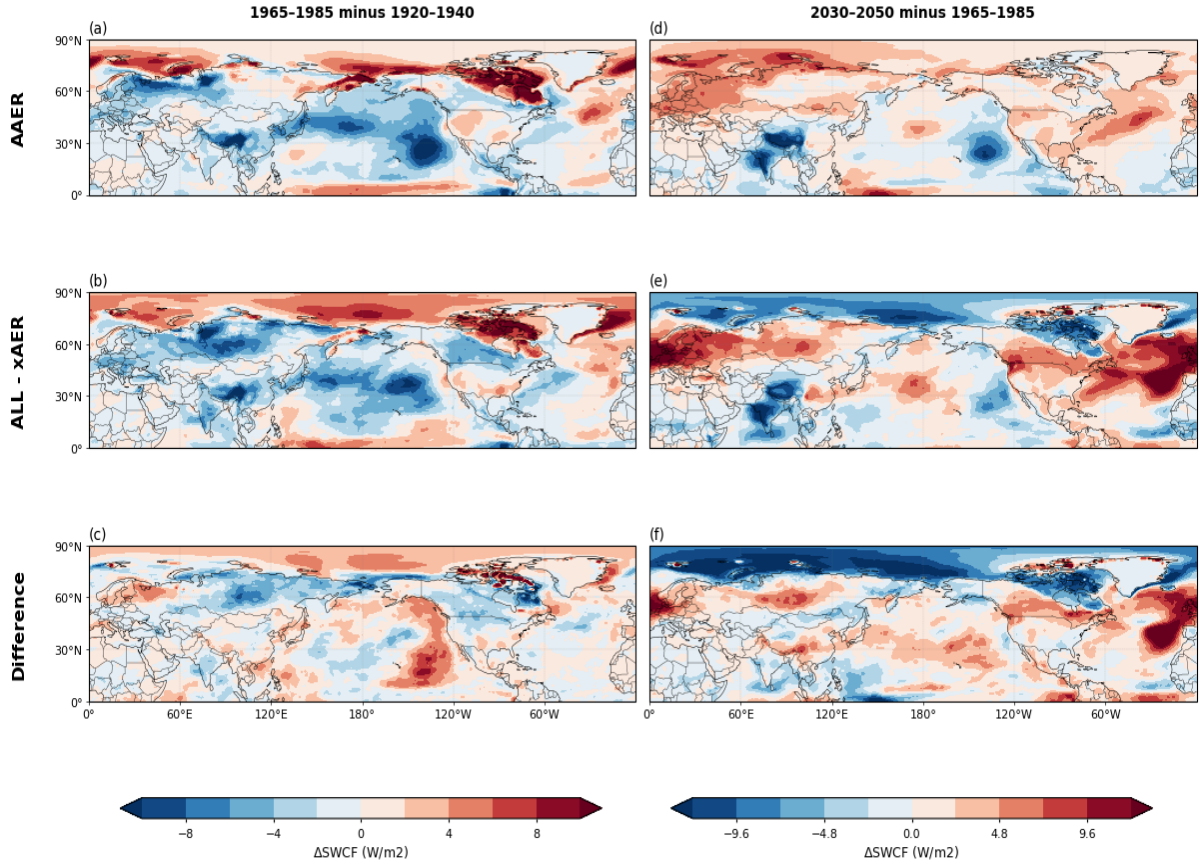

Figure S10. Changes in JJA mean shortwave cloud radiative effect (SWCF; shading, unit: W m^{-2}) between two different periods: 1965–1985 relative to 1920–1940 (left) and 2030–2050 relative to 1965–1985 (right) for the (a), (d) AAER, (b), (e) ALL−xAER, and (c), (f) difference between them (ALL−xAER minus AAER). Positive anomalies indicate a weakening of the shortwave cloud-cooling effect, whereas negative anomalies indicate a strengthening of the shortwave cloud-cooling effect.

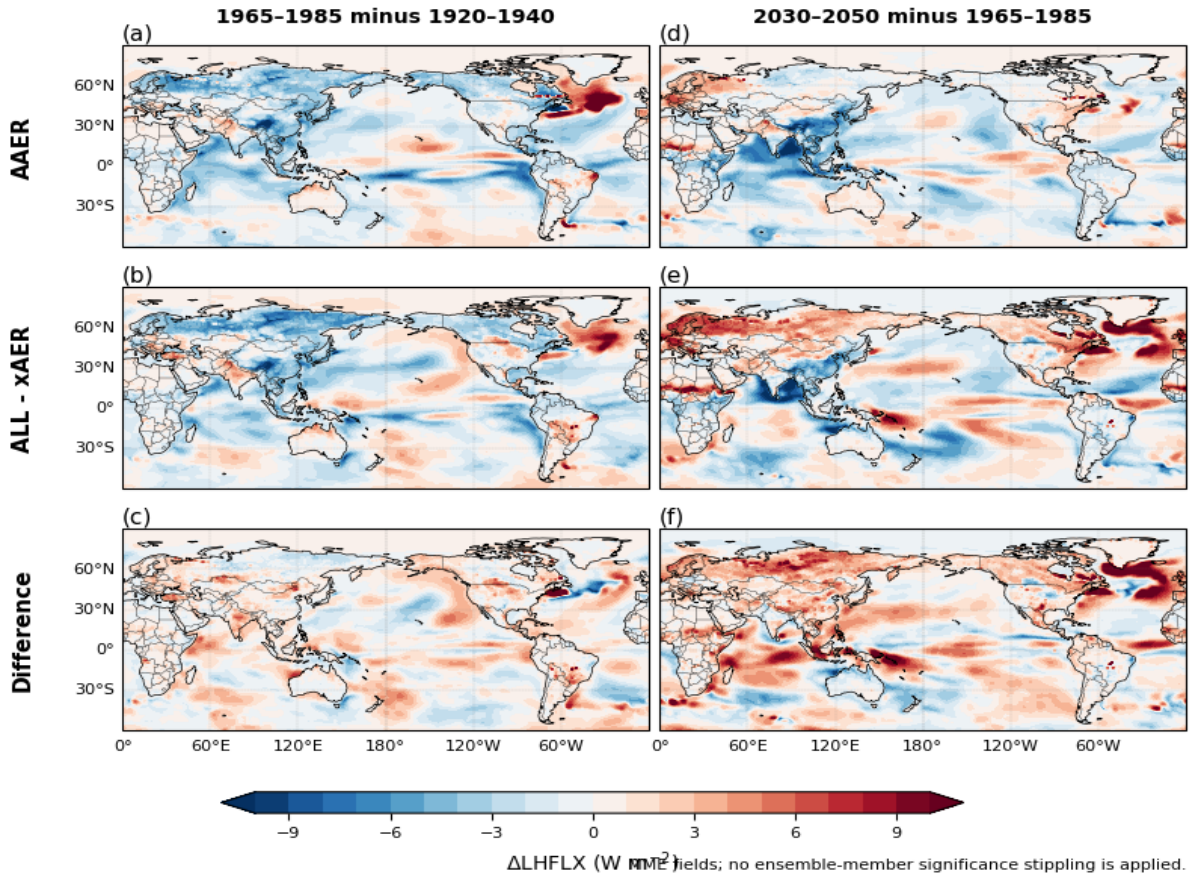

Figure S11. Changes in JJA mean surface latent heat flux (LHFLX; shading, unit: W m^{-2}) between two different periods: 1965–1985 relative to 1920–1940 (left) and 2030–2050 relative to 1965–1985 (right) for the (a), (d) AAER, (b), (e) ALL−xAER, and (c), (f) difference between them (ALL−xAER minus AAER). Positive anomalies indicate enhanced upward latent heat flux from the surface to the atmosphere under the CESM sign convention.